Taylor & Francis
Taylor & Francis Group

Automatika

Journal for Control, Measurement, Electronics, Computing and Communications

ISSN: (Print) (Online) Journal homepage: www.tandfonline.com/journals/taut20

Design, FEM analysis and development of switched reluctance motor electric drive for TRI-wheeler E-vehicle application

M. Anand, S. Jebarani Evangeline, W. Deva Priya & S. Chitra Selvi

To cite this article: M. Anand, S. Jebarani Evangeline, W. Deva Priya & S. Chitra Selvi (2024) Design, FEM analysis and development of switched reluctance motor electric drive for TRI-wheeler E-vehicle application, Automatika, 65:3, 813-829, DOI: 10.1080/00051144.2024.2330281

To link to this article: https://doi.org/10.1080/00051144.2024.2330281

Published online: 25 Mar 2024.

AUTOMATIKA
2024, VOL. 65, NO. 3, 813–829
https://doi.org/10.1080/00051144.2024.2330281

Design, FEM analysis and development of switched reluctance motor electric drive for TRI-wheeler E-vehicle application

M. Anand[a], S. Jebarani Evangeline[b], W. Deva Priya[c] and S. Chitra Selvi[d]

[a]Department of Electrical and Electronics Engineering, PSG College of Technology, Coimbatore, India; [b]Department of Electrical and Electronics Engineering, SNS College of Engineering, Coimbatore, India; [c]Department of Computer Science and Engineering, Saveetha School of Engineering, Saveetha Institute of Medical and Technical Sciences (SIMATS) University, Saveetha University, Chennai, India; [d]Department of Electrical and Electronics Engineering, University College of Engineering – Dindigul, (A constituent college of Anna University-Chennai), Dindigul, India

ABSTRACT

Electric vehicles have seen substantial growth in recent years in the emerging economies of the world. The current market scenario of E-vehicles is dominated by PMSM or BLDC motors due to their higher torque-to-power density, and efficiency with added performance metrics of the motor. However, the higher capital cost of permanent magnets makes the motor designers to consider an alternative to magnetic motors, the so-called Switched Reluctance Motors (SRM). With proper FEM analysis and controller design, if SRMs can able to achieve the performance metrics of a PMSM/BLDC, it will be a breakthrough in the automotive sector with affordable prices. Based on the aforementioned facts, this research work focuses on SRM as a viable alternative to the existing PMSM/BLDC motor. The work concentrates on the design and development of an 8/6 SRM for a Tri-wheeler E-vehicle application. The designed motor is fabricated, tested and controlled by WAVECT, an FPGA-based real-time digital controller which is used to control the commutation of the 8/6 SRM. The yielded response satisfactorily proves that the designed 8/6 SRM can be effectively used for the Tri-wheeler E-vehicle application, thereby paving the way for sustainable energy conservation in the automotive sector.

ARTICLE HISTORY
Received 12 January 2024
Accepted 8 March 2024

KEYWORDS
Electric vehicle; switched reluctance motor; permanent magnet synchronous motor; brushless direct current motor; WAVECT; field programmable gate array

Nomenclature

A_{sp}	pole area of the stator
D	inner diameter of the stator
L	stack length
β_s	pole arc angle of the stator
C	thickness of the back iron
A_y	area of the yoke
h_{sp}	pole height of the stator stamping slot
D_o	outer diameter of the stator
A_r	pole area of the rotor
g	air gap length
β_r	pole arc angle of the rotor
A_{rc}	core area of the rotor
h_r	pole height of the rotor stamping slot
D_{sh}	outer diameter of the shaft
A_g	area of the air gap
F_A	force to overcome the aerodynamic drag
c	nose form factor
S	cross sectional of the windward area
ρ	density of the air
V_R	relative velocity
P_A	power to overcome the aerodynamic drag
F_R	force to overcome the rolling resistance
f	force
m	mass of the vehicle
G	gravitational constant
P_R	power to overcome the rolling resistance
F_m	force to overcome acceleration
a	acceleration
P_M	power to overcome acceleration force
V_{rpm}	RPM of the SRM
T	rated torque of the SRM
P	rated power output of the SRM
ω	angular Velocity

1. Introduction

Transportation is the basic need for human beings to move from one place to the other. Due to the shortfall in fossil fuels, the cost price factor involved in transportation is increasing steadily day-by-day. Several countries of developed and emerging economies are proposing E-vehicles as an alternative to the traditional fossil fuel-based transportation economy. The E-vehicles take the first mover advantage with various performance metrics such as carbon-free emission, lower running and maintenance costs, free from noise pollution, ease of charging at home and overall coming with an exclusive

CONTACT M. Anand and.eee@psgtech.ac.in Department of Electrical and Electronics Engineering, PSG College of Technology, Coimbatore, Tamilnadu, India

tax and financial benefits which makes them as user and environmentally friendly. In countries like India, the growth is driven by various developments in the automotive sector and also the policies of the government in the promotion of E-vehicles for sustainable energy management.

The prime mover of the E-vehicle is the electric motors. Traditionally, the electric motors for e-vehicle applications are made of PMSM or the BLDC for the 2-wheeler and the 3-wheeler segments. The PMSM or the BLDC consists of the stator and the rotor. The stator houses the winding part and the rotor houses the magnets. The rotor may be of a surface permanent magnet type or the interior permanent magnet type. The magnets are made of Samarium cobalt (SmCo) or the neodymium–iron–boron (NdFeB) type of magnets which are primarily used to achieve a high torque-to-power density ratio with an enhanced high efficacy for the given volumetric and diametric constraints of the motor [1,2].

However, the cost associated with the permanent magnets and their environmental impact is a huge concern for the E-vehicle manufacturers and also the consumers which makes way for the motor designers to think of an alternative motor to the PMSM or the BLDC, which should be substantially free of permanent magnets, the so-called Switched Reluctance Motors [3]. SRMs have a gained a significant importance in the traction system due to its associated performance metrics such as the absence of copper conductors on the rotor, the absence of magnets, the robust rotor, and high fault tolerance with ease in mechanical maintenance and construction.

The Reluctance Motor and the Switched Reluctance Motor both operate on the principle of magnetic reluctance, however in SRM the magnetic path is intentionally varied using power electronics for high precision control for efficient and smoother operation with the magnitude and timing of the current pulses injected to the stator windings and hence SRM features higher torque density relative to their size and weight compared with the reluctance motors.

The feasibility of the SRM for the E-vehicle applications along with various drive topologies and the power trains was discussed in the literature [4]. The study concludes with state-of-art analysis that there exists a potential for SRM in the future E-vehicle market segments and formulated the future research perspectives for SRMs. The choice of multiphase SRM for E-vehicle application was presented in the literature [5]. The review takes into consideration various metrics such as converter topologies, winding topologies and various control drive aspects of SRMs which have been broadly summarized.

The design feasibility of SRMs for In-wheel E-vehicle applications was discussed in the literature [6]. A multi-objective function was defined to optimize the performance metrics of the SRM which comes at 16/20 In-wheel configuration of 96 V, 4 kW and rated speed of 1000 r/min. The simulated results validate the effectiveness of the proposed design. The design of SRM using the multi-objective function for E-vehicle applications was presented in the literature [7]. The SRM considered is a 12/10 SRM, 850 W of 6000 r/min for which the thermal and electromagnetic performance is presented. The simulated results have been validated with the hardware prototype which confirms the effectiveness of the proposed design.

The design feasibility of an SRM for E-vehicle propulsion application was presented in the literature [8]. The design approach of 3-phase, 4-phase and 6-phase SRM is studied using the FEM analysis. The study concludes that 4-phase SRM is viable when compared to the other designs for the E-vehicle propulsion application. The design and simulation of a 12/8 4 kW SRM for E-vehicle Tri-wheeler application were presented in the literature [9]. The study compares the electromagnetic performance metrics of the proposed SRM using the Ansys/Maxwell software package. The fact that the SRMs are an attractive technology for E-vehicle applications is validated in the literature [10]. Two types of SRM, a 12/16 for an e-bike application and the other 24/16 SRM for a traction application were designed, tested and validated and the test results confirm that the SRMs are a viable alternative solution to the existing permanent magnet motors and SRMs have a huge potential for E-vehicle applications.

The feasibility of an In-wheel SRM for low-power E-vehicle application was presented in the literature [11]. The SRM under consideration is 3-phase, 48 V, 835 rpm with a rated power of 1 kW. The test results are validated with the simulated ones which defends the effectiveness of the proposed methodology. The control of SRM using the direct torque control method and its feasibility are discussed in the literature [12]. The SRM considered is a 12/8 configuration of 30 V_{DC}, rated speed of 300 r/min and a load torque of 0.6 Nm. The simulated results are validated with the hardware prototype. The method of improving the efficiency and minimization of the torque ripple for a 4-phase 8/6 SRM is discussed in the literature [13]. The proposed method utilizes the modified direct-torque-control strategy and its effectiveness is validated with the hardware prototype results.

The SRM can achieve higher levels of torque with a lower magnitude of current when compared with the BLDC motors with similar operating conditions because the SRMs operate based on the principle of magnetic reluctance whereas the BLDC principle is based on the Lorentz force. The absence of permanent magnets in SRM reduces its rotor inertia and enables a compact, lightweight design leading to higher power density. The SRMs' simpler rotor construction with no windings and magnets in the rotor and with

reduced eddy current losses contribute to higher efficacy. Also, SRMs are inherently robust and durable due to the merits of the above-mentioned rotor construction which results in improved reliability compared with the BLDC motor under harsh operating conditions [14–16]. These factors pitch for a directive towards the EV application which requires a higher torque-to-current ratio since these are primarily powered by the battery-powered devices, and with an enhanced power density, efficacy and inherent robustness.

2. Research questions

A detailed literature survey has been presented in the aforementioned section, bringing out the works related to the SRM for E-vehicle applications. The SRMs come with various positive metrics such as the absence of magnets, absence of copper conductors on the rotor, robust rotor and high fault tolerance with ease in mechanical construction and maintenance. It is inferred that though SRMs potential has been validated for the In-wheel applications, there exists limited research work pertaining to the use of SRM for Tri-wheeler applications. There exists a research gap for the suitability of SRMs for Tri-wheeler applications since the SRMs are bound to fit within the required frame size for delivering the rated power and torque characteristics. Also, battery-operated Tri-wheeler-based E-vehicle applications haves seen a rising demand in many transportation systems. In the context of the aforementioned potentials, this research work aims at designing and developing an SRM for a Tri-wheeler-based E-vehicle application and its associated embedded control strategy to deliver an optimal electromagnetic performance of the machine. The work presented here will be useful to the research community who are working for an SRM for Tri-wheeler-based E-vehicle applications. The research work presented here provides insights and answers to the following research questions.

1. Whether the SRMs are suitable for Tri-wheeler based E-vehicle applications?
2. Can the SRMs be a potential replacement for PMSM or BLDC?
3. Can SRMs be a low-cost choice for Tri-wheeler E-vehicle applications?
4. Shall the SRMs deliver the optimal efficiency at higher temperatures?
5. Can the SRM accommodate the high torque and power density within the given frame size?

3. Design methodology of SRM

The dimensional metrics of the SRM considered for the E-vehicle application are sized based on the major geometrical constraints, namely the outer diameter of the stator, the inner diameter of the stator, outer diameter of the rotor, the inner diameter of the rotor and the stack length with suitable iterations of the stator and the rotor pole arc angles [17,18]. The pole area of the stator is determined by Equation (1) which is the same as that of the area of the yoke

$$A_{sp} = D \times L \times \frac{\beta_s}{2} \tag{1}$$

The back-iron thickness of the stator is calculated using Equation (2)

$$C = \frac{A_y}{L} \tag{2}$$

The pole height of the stator stamping slot is determined by Equation (3) and the pole area of the rotor is determined by Equation (4).

$$h_{sp} = \frac{D_O}{2} - C - \frac{D}{2} \tag{3}$$

$$A_r = \left(\frac{D}{2} - g\right) \times L \times \beta_r \tag{4}$$

The core area of the rotor is determined by Equation (5) and the pole height of the rotor stamping is determined by Equation (6).

$$A_{rc} = \frac{A_{sp}}{1.6} \tag{5}$$

$$h_r = \frac{D}{2} - g - \frac{D_{sh}}{2} - \frac{A_{rc}}{L} \tag{6}$$

The area of the air gap is determined using Equation (7).

$$A_g = \left(\frac{D}{2} - \frac{g}{2}\right)\left(\frac{\beta_r + \beta_s}{2}\right) L \tag{7}$$

Following the equations as depicted in Equations (1)−(7), the preliminary sizing of the SRM is frozen and the electromagnetic performance of the SRM is computed using the FEM analysis [17,18]. If the machine requires optimal performance at the optimal load point, then the design dimensions are revisited and iterated such that the desired electromagnetic characteristics are yielded for the given frame size of the SRM.

Selecting the optimal stator/rotor pole configuration of the SRM is critical for EV applications. The number of stator poles may include 4, 6, 8, 10 or higher stator poles, and similarly the rotor pole configurations include 2, 4, 6, 8 or higher rotor poles and these combinations are determined by the desired key performance metrics. An 8/6 configuration shall yield good torque density, higher efficiency over a wider speed range and reduced torque ripple when compared with the 6/4 configuration and similarly higher stator poles like 12/8 may result in additional phase winding which results in additional power electronic switches for commutation

and expensive manufacturing costs. Hence, the 8/6 stator/rotor pole configuration is selected as the optimal stator/rotor pole configuration of the SRM based on the aforementioned performance metrics.

4. Sizing the power rating of the SRM

The required force to overcome the aerodynamic resistance is computed using Equation (8) and the power required to overcome the aerodynamic resistance is determined using Equation (9) [19].

$$F_A = \frac{C \times S \times \rho}{2} \times \frac{V_R{}^2}{3.6^2} = 24.55\ \text{N} \tag{8}$$

$$P_A = 24.55 \times 11.11 = 272.75\ W \tag{9}$$

The required force to overcome the rolling resistance is computed using Equation (10) and the power required to overcome the rolling resistance is determined using Equation (11).

$$F_R = fmg\cos\alpha = 43.28\ \text{N} \tag{10}$$

$$P_R = 43.28 \times 11.11 = 480.84\ \text{W} \tag{11}$$

The required force to overcome the acceleration is computed using Equation (12) and the power required to overcome the acceleration force is determined using Equation (13).

$$F_M = m\text{a} = 274\ \text{N} \tag{12}$$

$$P_M = 274 \times 11.11 = 3044.14\ \text{W} \tag{13}$$

The rate of change in voltage with time is determined using Equation (14).

$$\text{a} = \frac{dv}{dt} = 0.694 \tag{14}$$

The rated rpm of the switched reluctance motor is determined using Equation (15).

$$V_{rpm} = 9.549 \times \frac{V\left(\frac{m}{s}\right)}{r(m)} = 3000\ \text{RPM} \tag{15}$$

The shaft torque of the switched reluctance motor is determined using Equation (16).

$$T = \frac{P}{\omega} = 11.7\ \text{Nm} \tag{16}$$

The total shaft power output of the switched reluctance motor is determined using Equation (17).

$$\begin{aligned}\text{Total Power} &= P_A + P_R + P_M \\ &= 272.75 + 480.84 + 3044.14 = 3.79\ \text{kW}\end{aligned} \tag{17}$$

Table 1. Specifications of the SRM.

Parameter	Value	Unit
Shaft power output	3.7	kW
Rated voltage	220	V
Rated current	18.5	A
Number of stator poles	8	–
Number of rotor poles	6	–
Rated speed	3000	rpm
Rated torque	11.8	Nm
Stator outer diameter	165	mm
Stator inner diameter	90	mm
Rotor outer diameter	89	mm
Rotor inner diameter	33	mm

5. FEM analysis of SRM

The work starts with the electromagnetic modelling of the SRM for the power rating of 3.7 kW. The FEM analysis is carried out by the Ansys software which is an electromagnetic suite to predict the electromagnetic performance metrics of the SRM. The SRM considered for the design is given in Table 1. Negative torque in SRM needs appropriate mitigation as these can cause undesirable vibration and noise, particularly at low-speed levels. The mitigation of negative torque can be arrived at using current control strategies, precise rotor feedback estimation and appropriate commutation control of switches and optimized design geometry of the SRM. Optimizing the stator and rotor design geometrical parameters and their attributes is the most efficient and low-cost strategy for mitigating the effects of the negative torque in the SRM. The various dimensions are chosen based on the governing equations as listed in Equations (1)−(7), and the dimensions are revisited to achieve the required specific electric and magnetic loading of the SRM at the optimally loaded conditions with maximum efficiency at the rated conditions.

The speed−torque characteristics of the SRM are depicted in Figure 1. It is evident that the designed SRM has the required high starting torque to propel the vehicle as depicted in Figure 1. The SRM delivers the rated shaft power output of 3.7 kW at the rated speed of 3000 rpm as depicted in Figure 2. The efficiency of the SRM seems to be greater than 87% as seen in Figure 3 which concludes the optimal performance metrics of the designed SRM. Also, based on the flux linkages with variations in current as shown in Figure 4, the magnetic flux density plots as shown in Figure 5 and the magnetic flux lines as shown in Figure 6, it is evident that the SRM lies within the safe boundary limits of the guideline values for the flux density's such that the core of the SRM does not undergo magnetic saturation. The magnitude of the flux linkage of the SRM at the individual phases is shown in Figure 7. The rated current plot at the rated speed conditions is obtained by the excitation of the 4-phases of the SRM, namely Phases A, B, C and D and its performance for the rotor angle and source phase angle is depicted in Figures 8 and 9, respectively. The FEM analysis concludes that the designed SRM meets

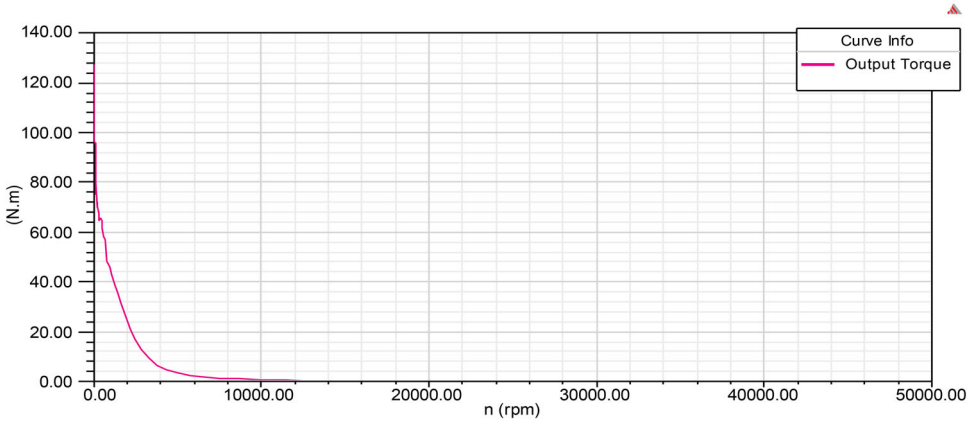

Figure 1. Torque vs speed characteristics.

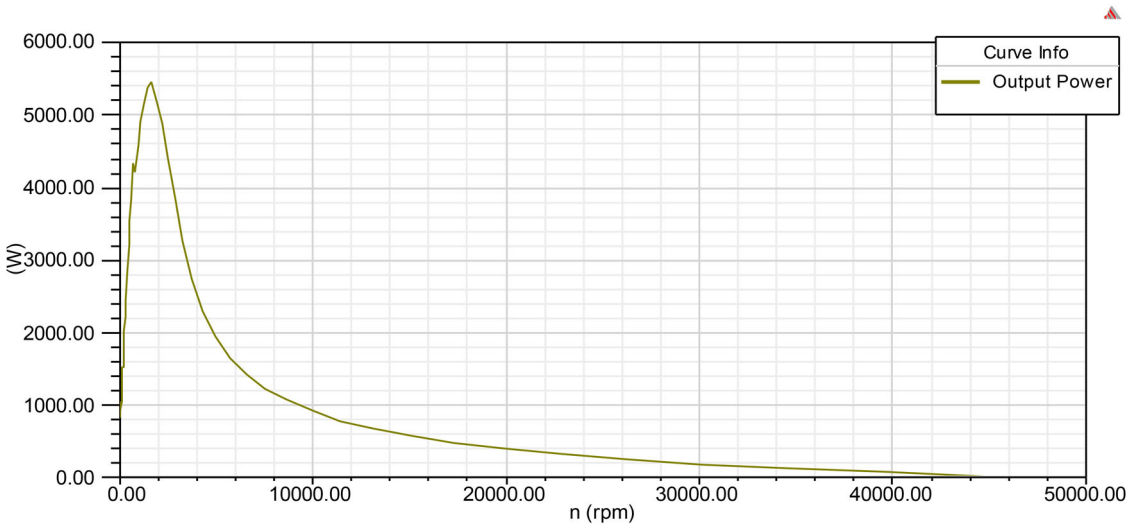

Figure 2. Output power vs speed.

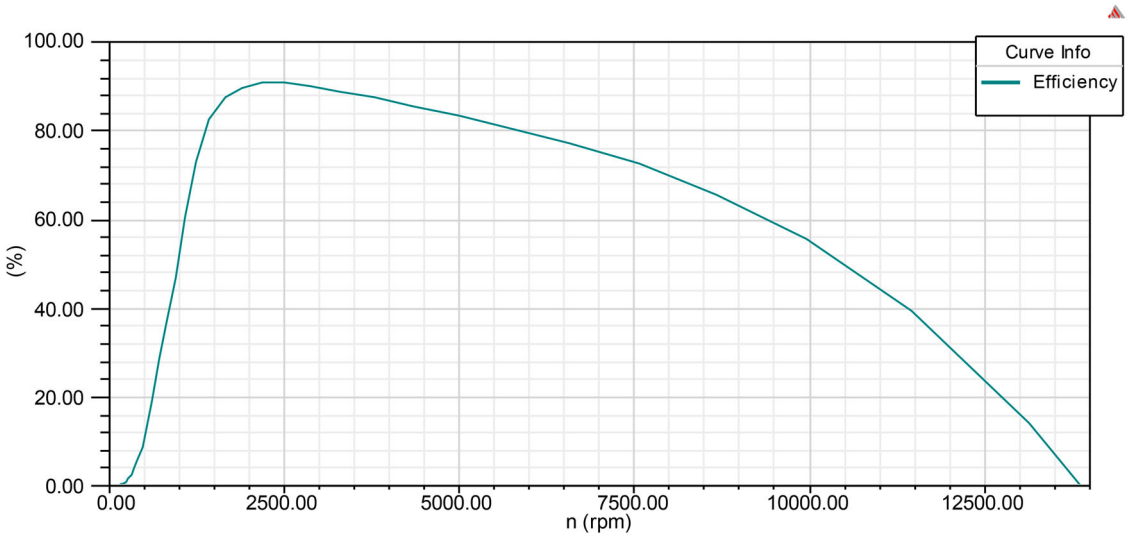

Figure 3. Efficiency vs speed.

the performance of the target E-vehicle application for the desired gradient and the electromagnetic plots also reveal that the SRM is suitably designed to handle the traction loading within the specified boundary limits.

6. Fabrication and control methodlogy of SRM

The prototype of the designed SRM is fabricated as per the standard conditions within the required frame size.

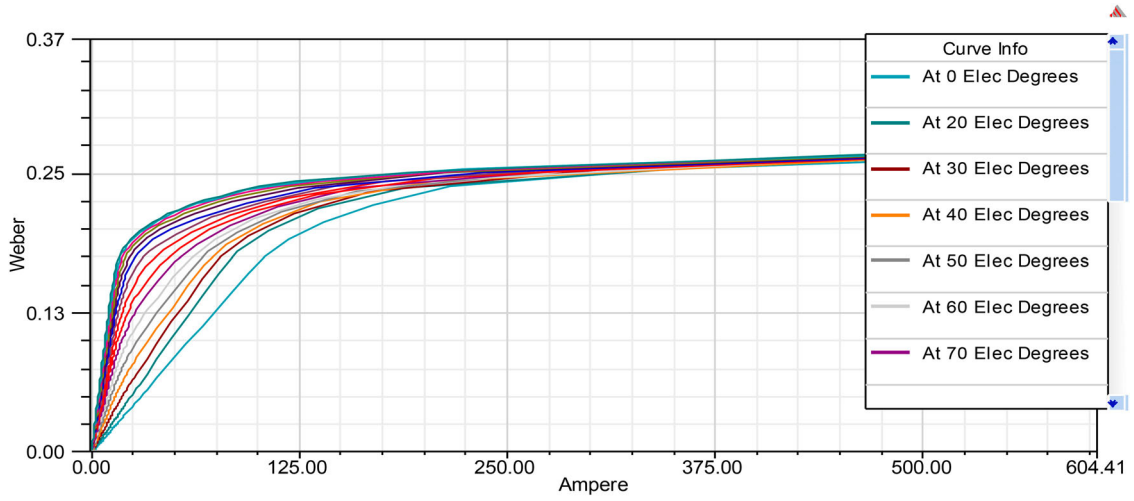

Figure 4. Flux linkage vs current.

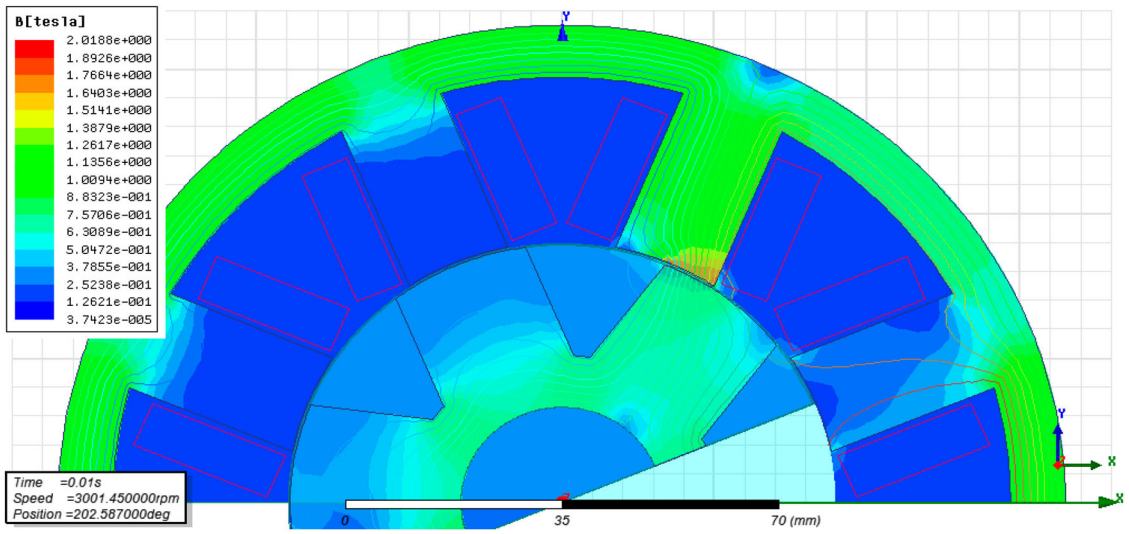

Figure 5. Magnetic flux density.

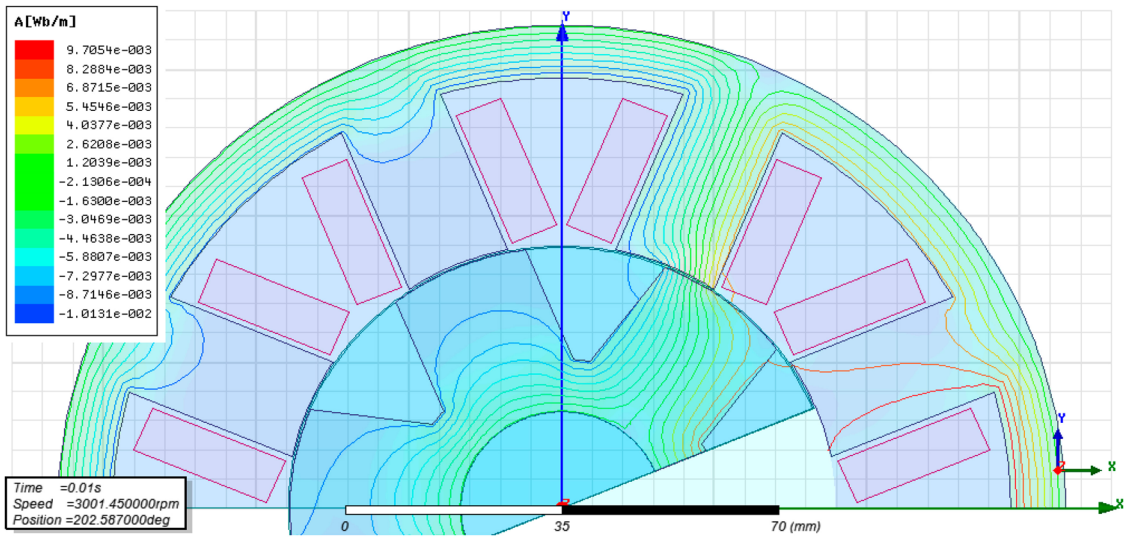

Figure 6. Magnetic flux lines.

The bearings of the SRM are selected to overcome the thermal overloading conditions. The SRM prototype is to be tested and controlled through the SEMIKRON converter based on the IR-based position sensors. The inductance profile of the SRM is the key feature that determines the commutation sequence of the IGBTs of the 4-legged DC-DC converter and hence proper testing is required to predetermine the value of the

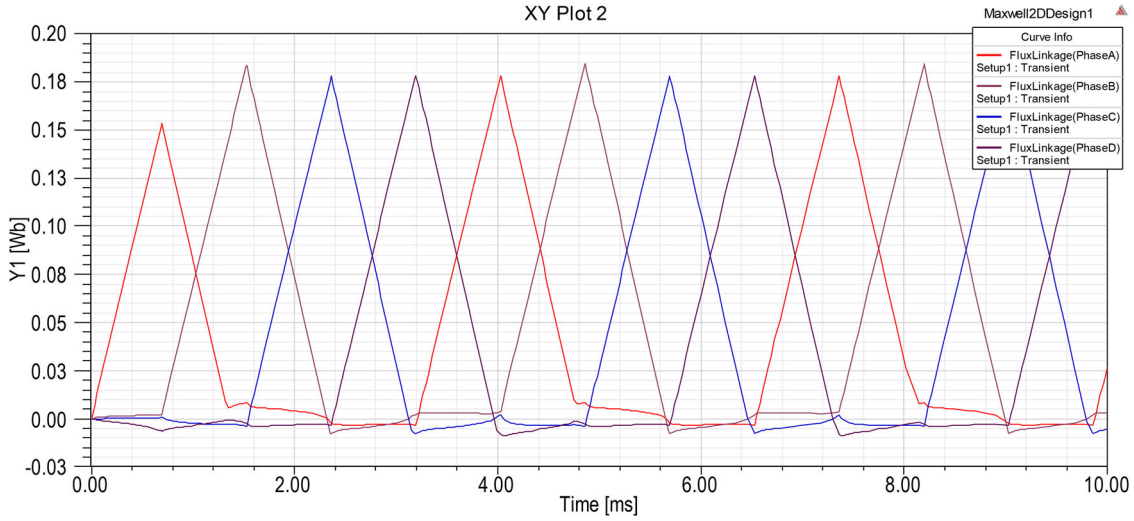

Figure 7. Flux linkages vs time.

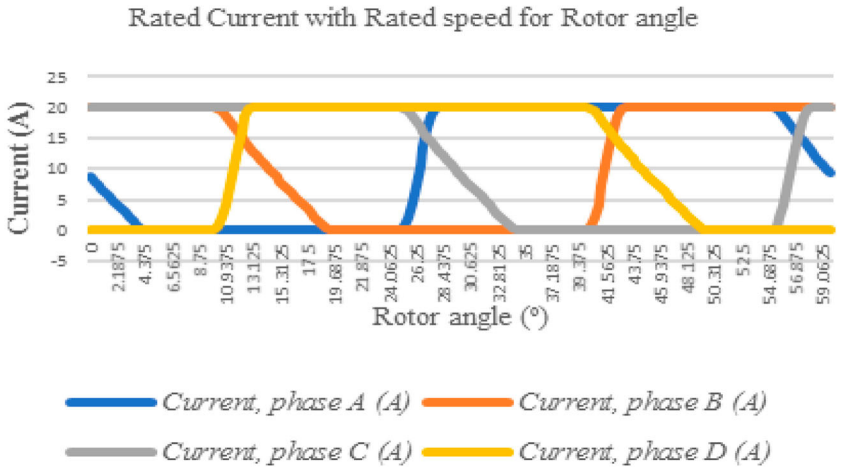

Figure 8. Rated current for rotor angle.

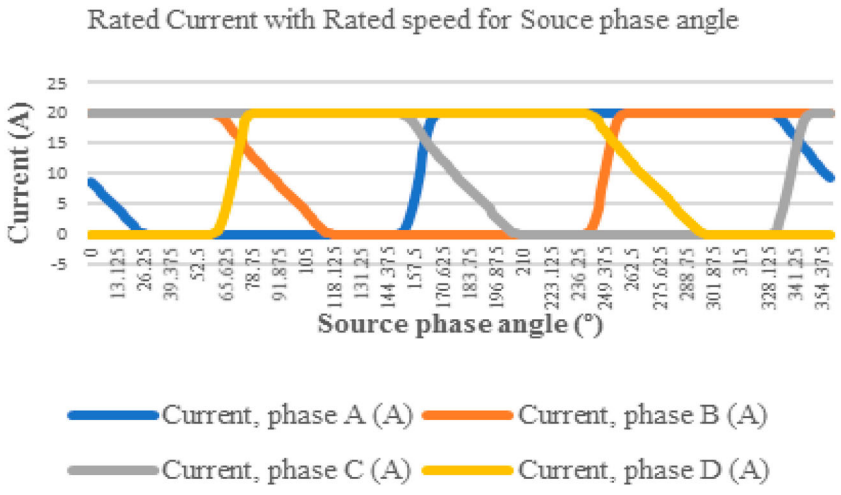

Figure 9. Rated current for source phase angle.

individual phase inductances to obtain a highly accurate commutation sequence for the SRM. The inductance profile of the SRM is measured using the LCR meter by rotating the shaft of the SRM periodically every 10 degrees. The encoder circuit (IR transmitter and receiver) is placed on the non-driving end of the shaft of the SRM which is suitably biased by 5 V DC supply and the inductance variations are recorded. Figure 10 shows the experimental set-up for the measurement of the inductance profile of the designed SRM.

Attaining an ideal inductance profile for an SRM is not feasible due to its inherent characteristics. The factors attributing to the non-ideal inductance profile

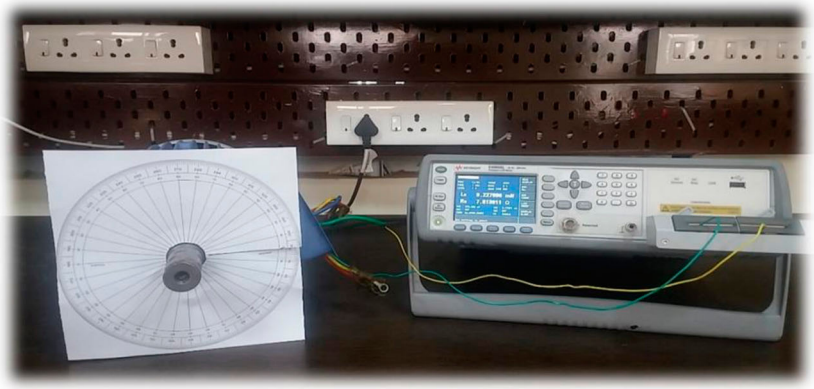

Figure 10. Inductance profile measurement using LCR meter.

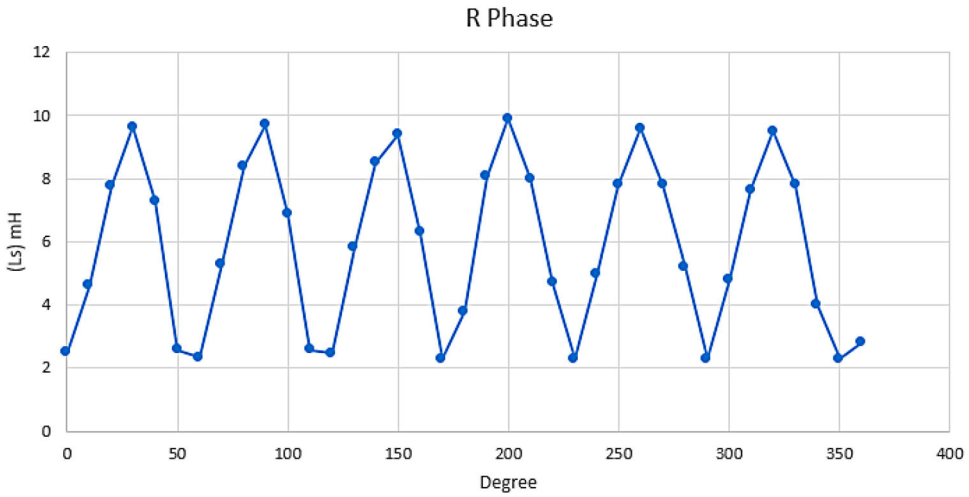

Figure 11. Inductance profile for R-phase of the SRM.

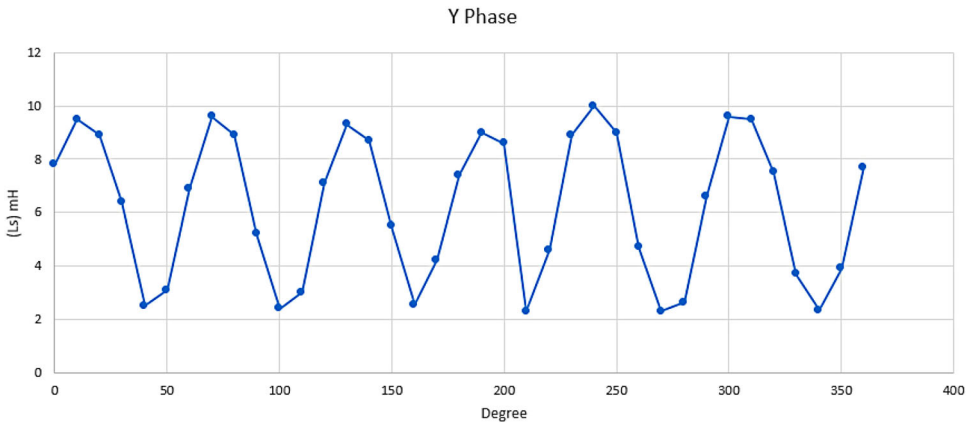

Figure 12. Inductance profile for Y-phase of the SRM.

are the variable inductance of each phase winding due to the rotor positions, non-linear characteristics due to magnetic flux path and geometrical shapes of stator/rotor poles, non-idealities of the magnetic materials due to hysteresis and eddy current losses, dynamics in switching and control complexity of the SRMs. The individual inductance variations of the phases R, Y, B and G are shown in Figure 11–14, respectively, and the consolidated inductance profile of the SRM is shown in Figure 15. The encoder response is also recorded when the inductance of the pole moves from the aligned to the unaligned position and it is depicted in Figure 16, which forms the basis for the commutation sequence of the SRM. Figure 17 shows the detailed view of the IR position sensors and their fabrication mechanism at the non-driving end of the shaft of the SRM.

The overall block diagram for the control of SRM is shown in Figure 18. A constant DC supply is obtained using the AC/DC uncontrolled rectification and the constant DC is fed to the DC-DC (classical asymmetric bridge converter) which consists of the IGBTs to obtain a pulsed DC which is then fed to the windings of the

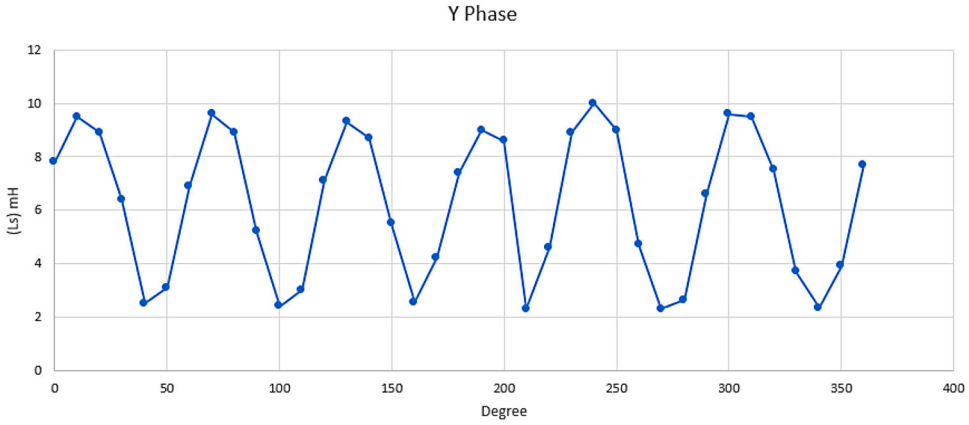

Figure 13. Inductance profile for B-phase of the SRM.

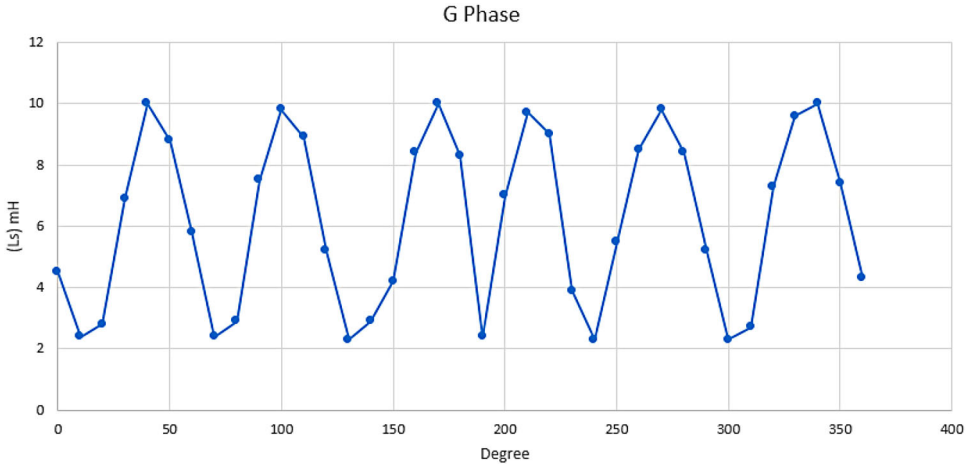

Figure 14. Inductance profile for G-phase of the SRM.

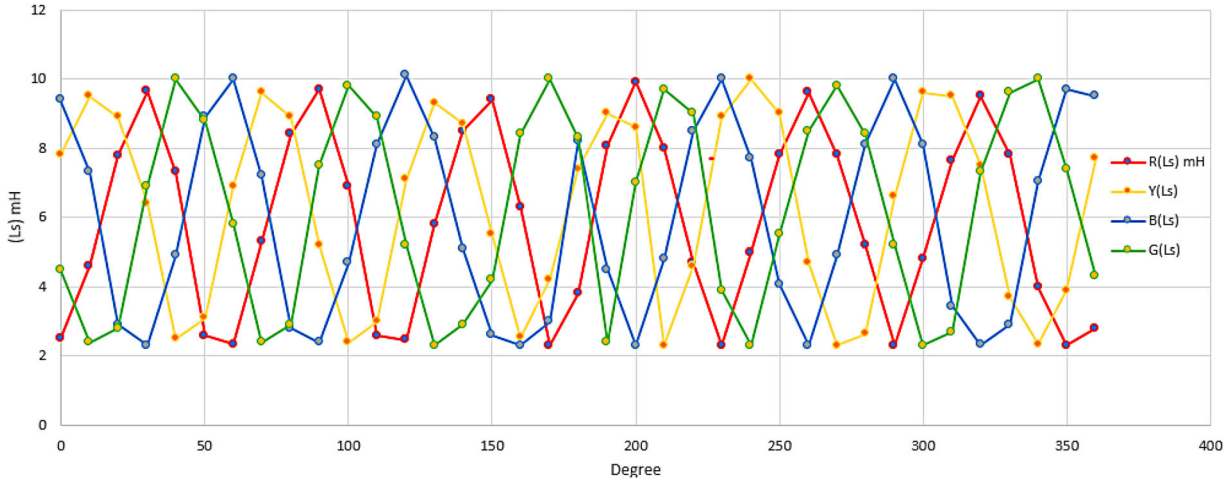

Figure 15. Consolidated inductance profile for the prototype SRM.

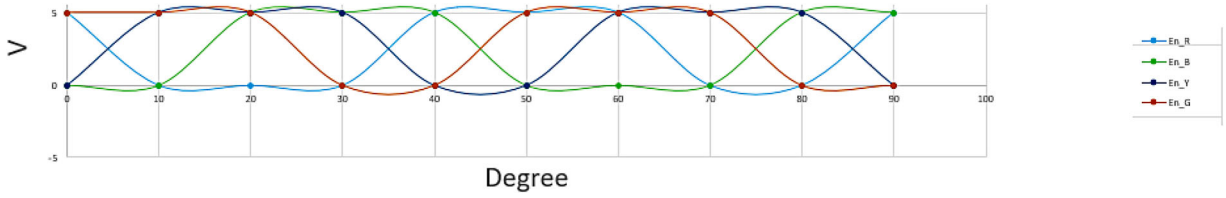

Figure 16. Consolidated response of the encoder of the SRM.

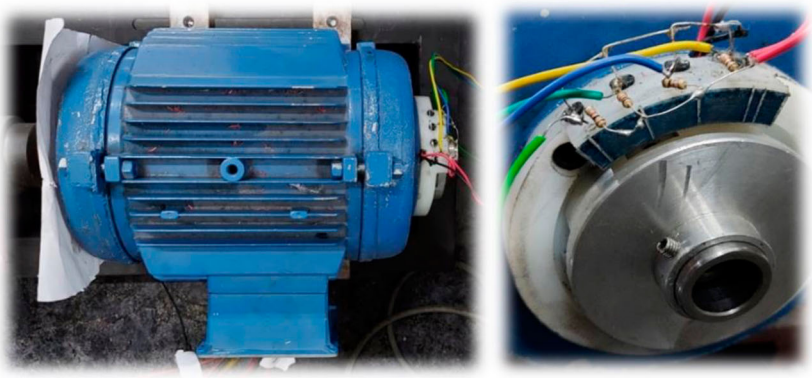

Figure 17. Encoder interfacing at the non-driving end of the SRM.

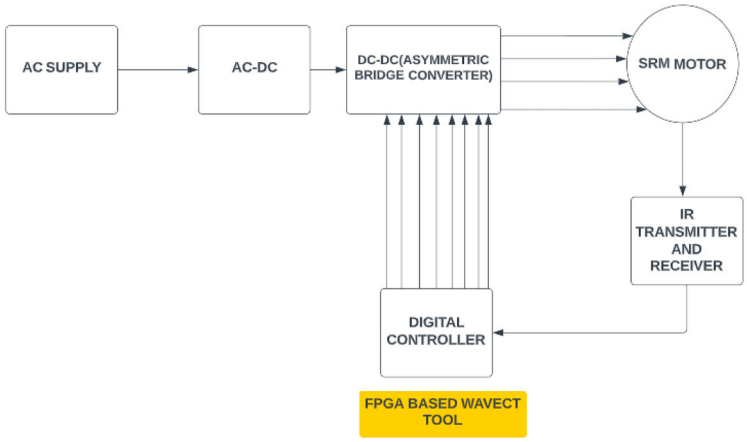

(a) Block Diagram of the Control of SRM

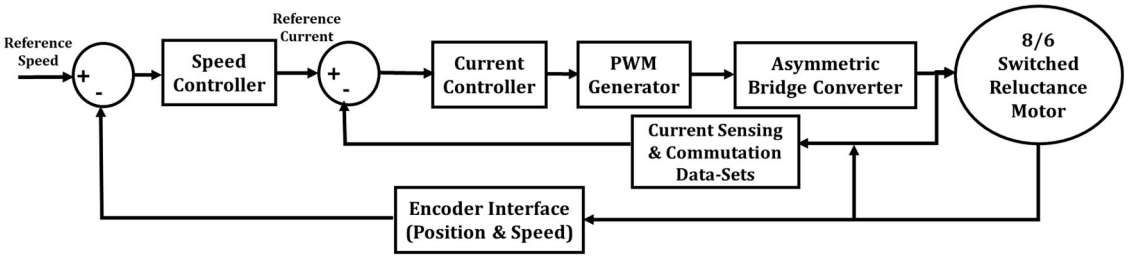

(b) Vector Control Block-Sets of SRM

Figure 18. Control strategy of 8/6 SRM. (a) Block diagram of the control of SRM and (b) vector control block-sets of SRM.

Figure 19. FPGA-based WAVECT real-time controller.

SRM. The control of SRM modelled in this research work involves capturing the position of the rotor using hall sensors as depicted in Figure 17. Typically, four hall sensors are used for the rotor position detection of SRM. The output of the hall sensors governs the inductance profile as depicted in Figure 15, which in turn controls the commutation sequence of the IGBT switches of the 4-legged DC-DC converter as shown in Figure 20. Hence, the controller can determine the exact position of the rotor relative to the stator phase

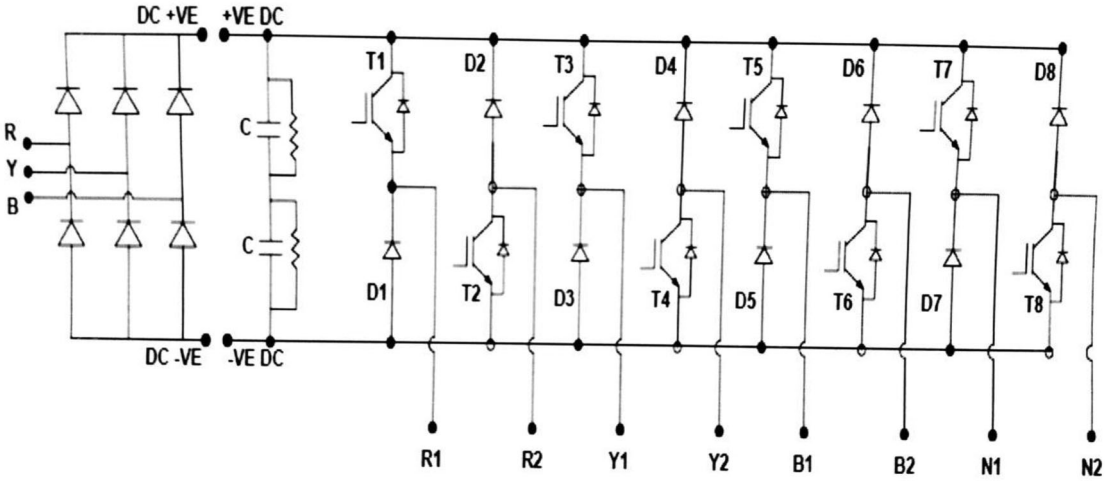

Figure 20. Power circuit configuration of the SEMIKRON stack for SRM control.

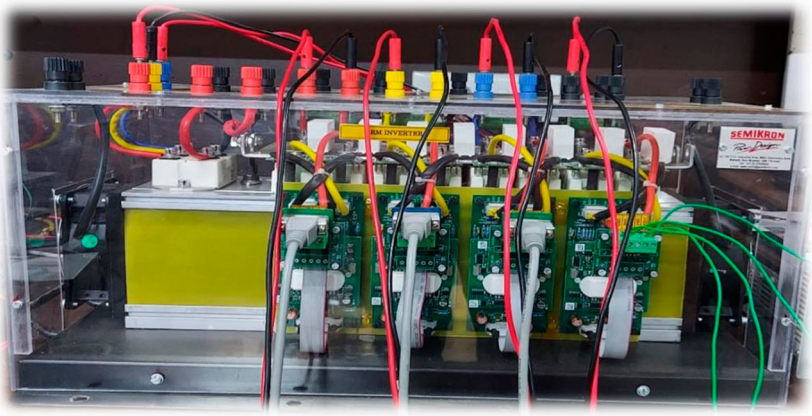

Figure 21. PWM control ports of the SEMIKRON stack for SRM control.

by monitoring the output of the hall sensors. This is attributed to energizing the appropriate phase winding, commutating the current flow from one phase to the other, synchronizing with the position of the rotor compensating for variations in speed, load and other operating conditions, thereby maximizing the torque production and its efficiency. The SRM utilizes the closed-loop control for the speed and torque control based on the measured variables such as the voltage, current, position and speed. The encoders fitted with the IR sensors are used to regulate the speed, position and excitation of the phase windings by a linear PI controller, whereas the current controller receives the current feedback from the current sensors which is utilized for the precise control of the shaft torque. Hence, an outer speed loop and an inner current loop with a torque controller are essential for the vector control of the SRMs. The controller chosen for the SRM is WAVECT which is a high-end FPGA-based real-time controller for fast rapid prototyping of the system with dynamic variations at the optimally loaded conditions. The WAVECT controller is depicted in Figure 19. The power circuit of the SRM is realized through the SEMIKRON stack which consists of AC/DC uncontrolled rectification at the front end and the DC/DC conversion using the classical asymmetric bridge converter at the second stage of the stack. The stack is well supported for voltage and current protections which forms an integral part of the loading of the SRM. The circuit configuration and the control terminals of the stack which are used for the control of SRM are depicted in Figures 20 and 21, respectively.

The driving end of the shaft of the SRM is coupled to the swinging field d.c. dynamometer which will be acting as the static load to the SRM. The field of the swinging field d.c. dynamometer is excited by a constant DC voltage source of 220 V. The frame of the swinging field d.c. dynamometer is pivoted to a load cell, from which the load torque of the SRM is obtained. A proximity switch is attached to the shaft of the armature of the swinging field d.c. dynamometer from which the speed of the SRM is measured. The speed and the torque sensors mounted on the swinging field d.c. dynamometer give the performance metrics of the SRM at the optimally loaded conditions. The complete test workbench set-up for the control of SRM is shown in Figure 22.

The SRM is controlled through the WAVECT which is integrated into MATLAB/Simulink. The Xilinx block sets are the control tool sets which are the FPGA-based control logic used for the fast commutation sequence

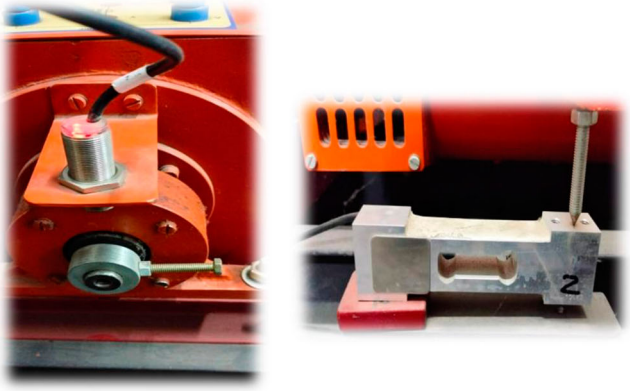

(a) Proximity Sensor and Load Cell Set-up

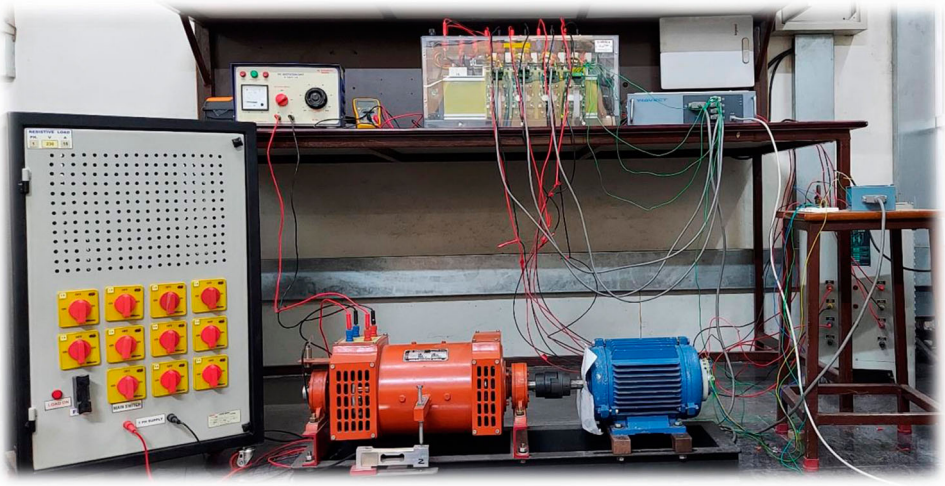

(b) Assembled Hardware Control Set-up

Figure 22. Test workbench set-up for the control of SRM. (a) Proximity sensor and load cell set-up and (b) assembled hardware control set-up.

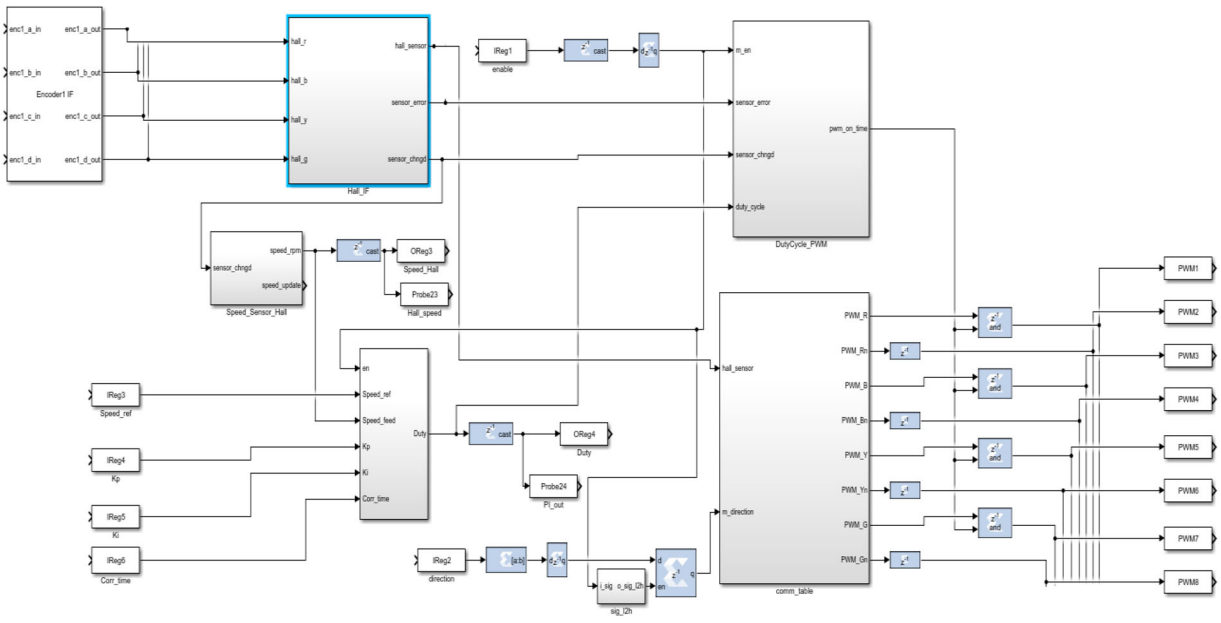

Figure 23. Control block sets of SRM in MATLAB/Simulink integrated to WAVECT.

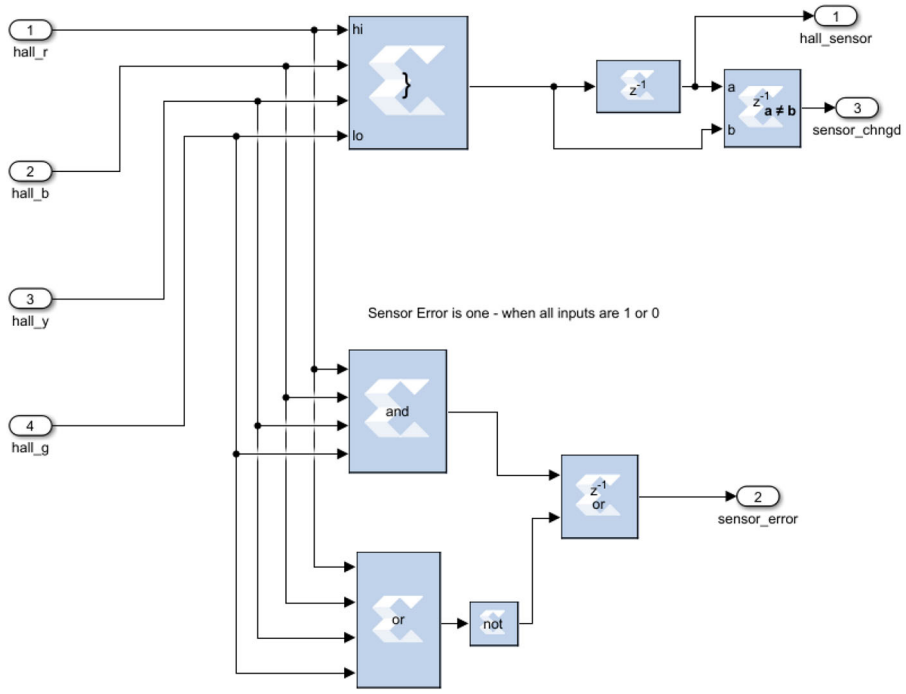

Figure 24. Control block sets of IR sensors for the encoder response.

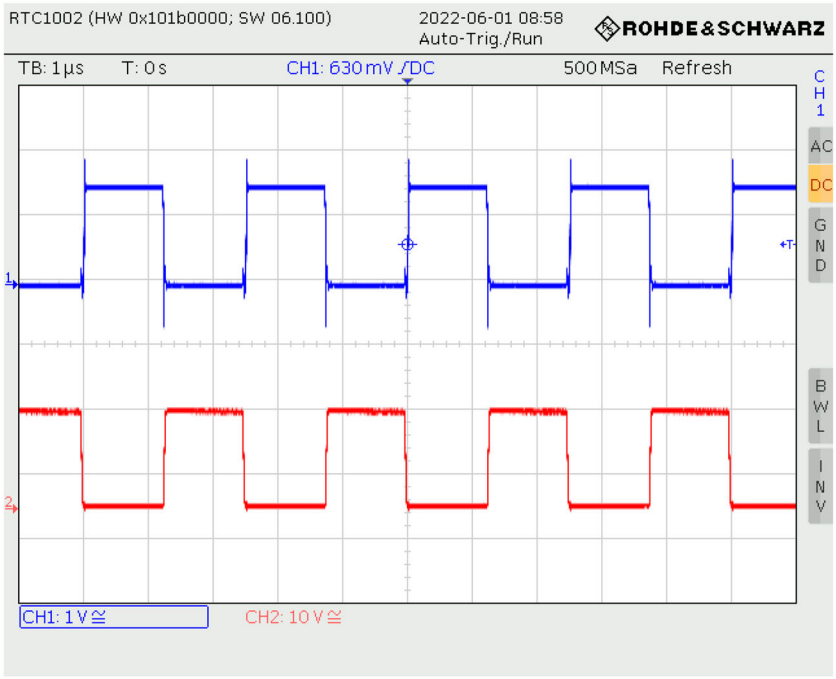

Figure 25. PWMs from the output ports of the WAVECT.

of the SRM based on the high-speed encoder response. The PWM signals of 8 numbers are generated based on the encoder response of the aligned and unaligned inductance profiles of the poles of the SRM and the response is validated with the look-up table which predetermines the phases of excitation of the SRM and accordingly the PWMs are triggered for the corresponding phases of the SRM. The overall control block of the SRM developed through MATLAB/Simulink which is integrated to the WAVECT real-time controller is shown in Figure 23. The block sets for the input/output configurations of the IR sensors for the encoder response are shown in Figure 24.

7. Hardware test results of SRM

The control strategy as depicted in Figure 23 is implemented using the WAVECT embedded controller and the SRM is subjected to the static load test using the swing field DC dynamometer connected to the resistive bank of lamp loads. The hall sensors depict the position of the rotor poles in relative displacement to

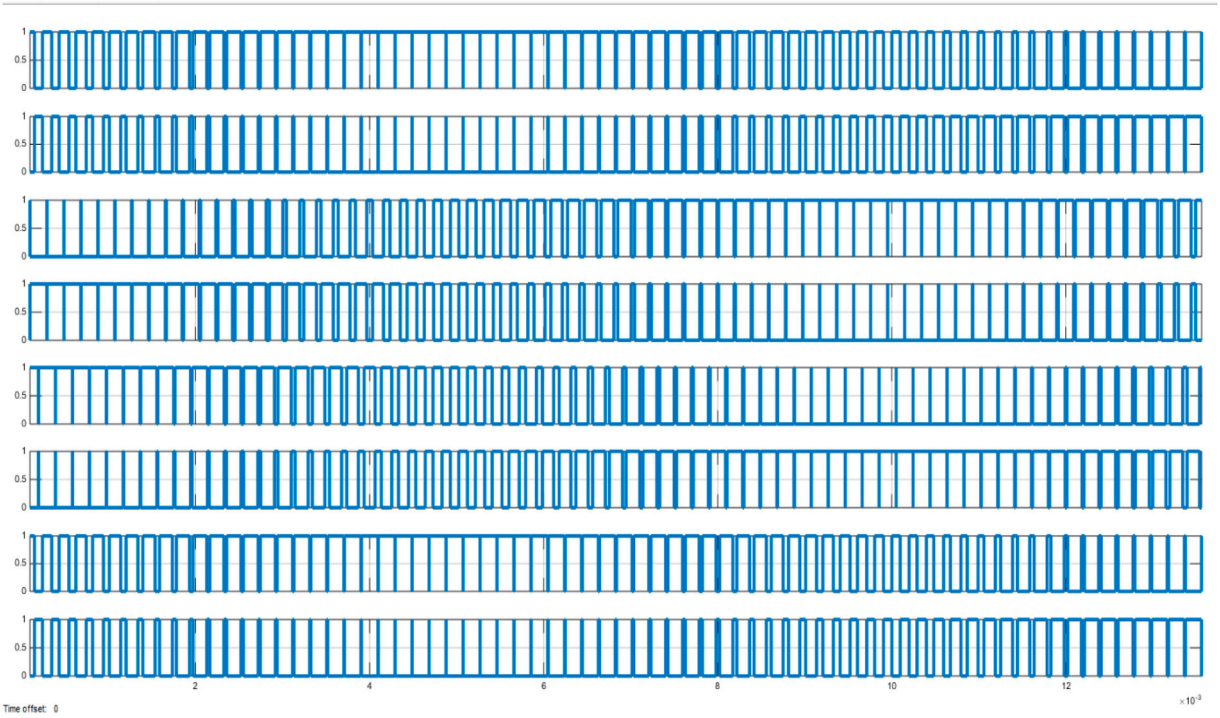

Figure 26. Consolidated 8 PWM signals for the SRM.

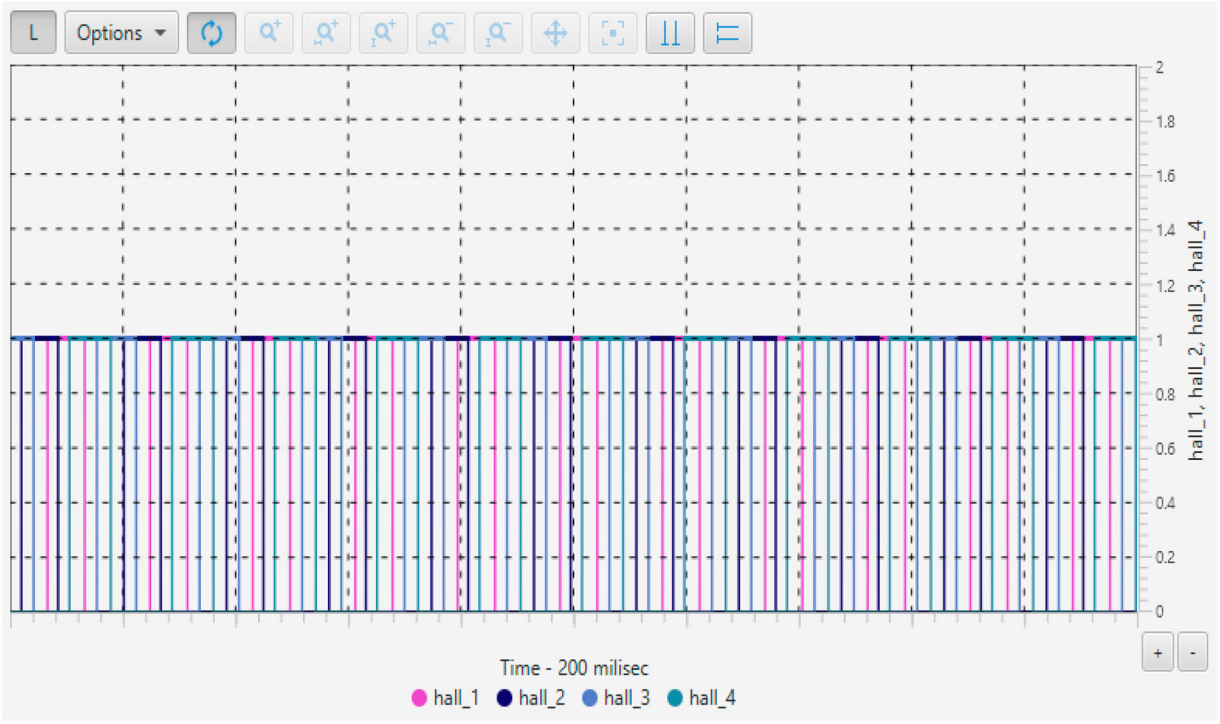

Figure 27. Signals of the IR sensors at a speed of 200 rpm.

the stator poles and according to the commutation table, the PWM signals are generated. The PWM signals generated through the WAVECT controller are shown in Figure 25. The consolidated 8 PWM signals are depicted in Figure 26. The response of the encoder is shown in Figure 27 for all the 4 IR sensors which are balanced for all 4 phases captured at a speed of 500 rpm. As the individual stator poles get excited sequentially, the currents are injected into the individual 4 phases and the consolidated current magnitude of the individual phases of R, Y, B and G is captured in Figure 28, which depicts that the magnitude of the instantaneous currents is almost balanced with the current ripple of less than 1.5% which lies within the boundary of permissible limits. Any change in the load dynamics is captured by the PI controller and the gains are regulated in closed-loop control yielding the required torque demand. The voltage across the individual 4 windings of the SRM is shown in Figure 29 which validates the effectiveness of the dv/dt

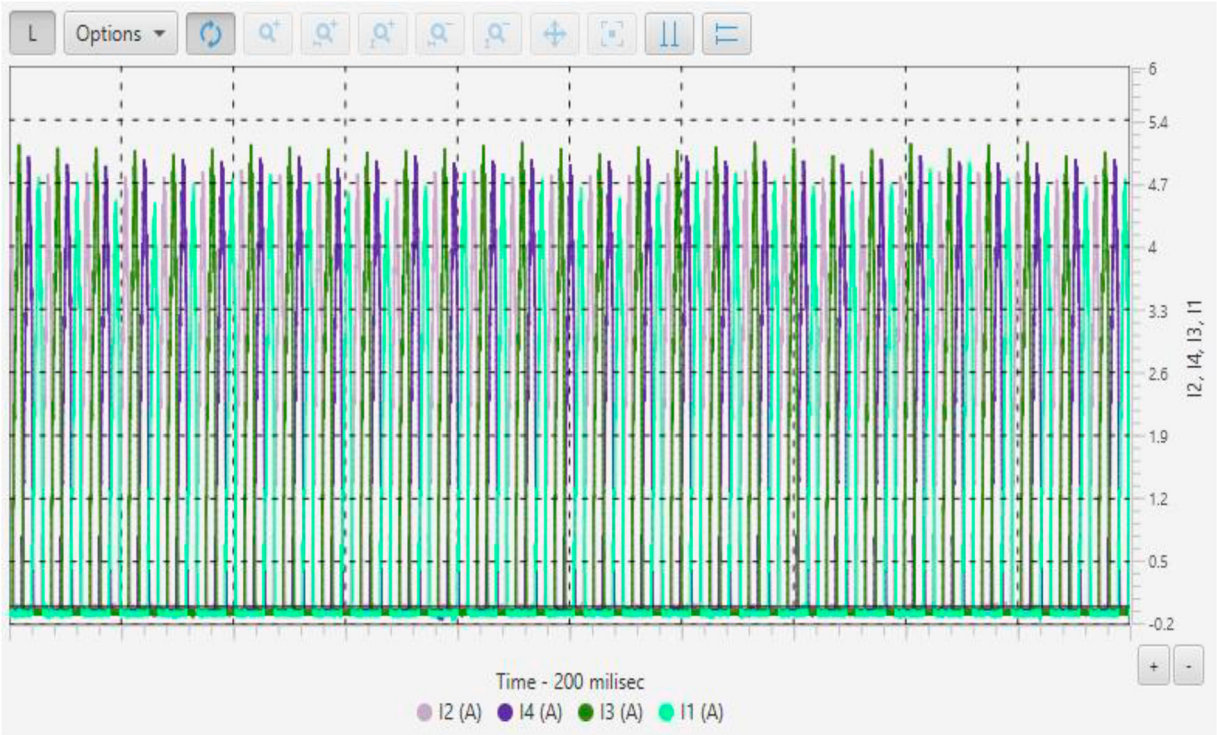

Figure 28. Signals of current sensors at a speed of 1500 rpm.

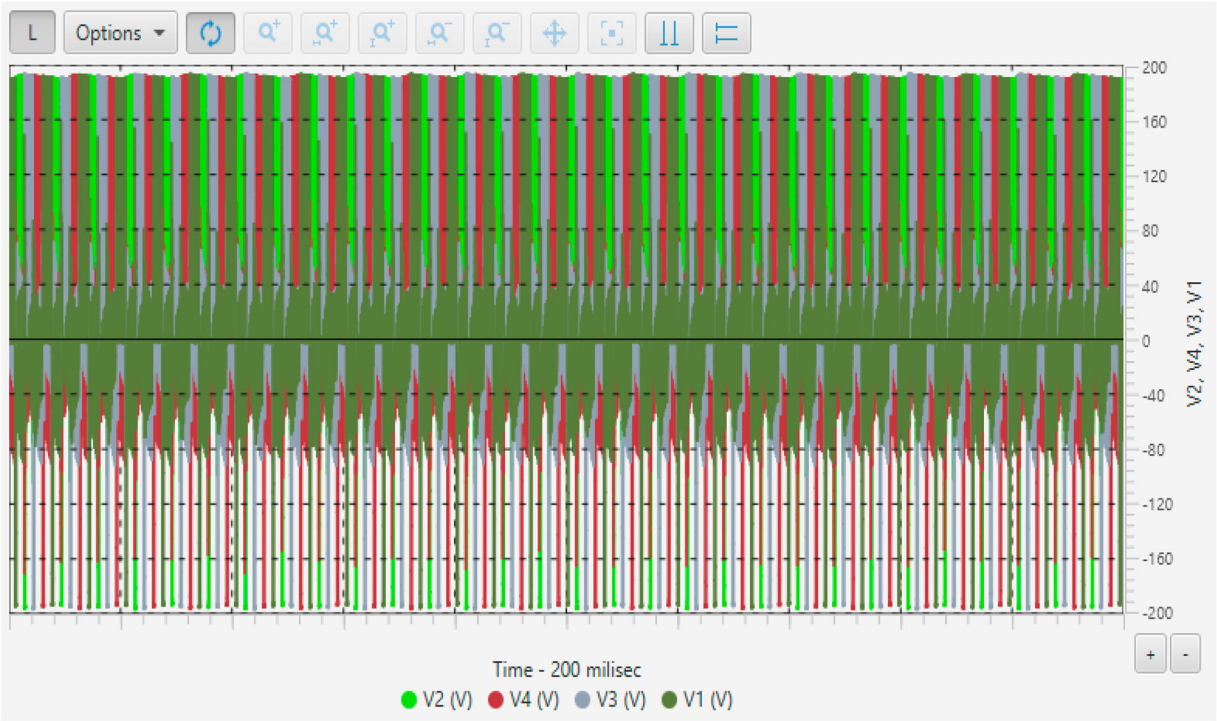

Figure 29. Signals of voltage sensors at a speed of 3000 rpm.

protection of the windings and IGBTs under the standard test conditions with the voltage ripple less than 5%. The machine is loaded for the rated condition and the current in the 4-phase windings at the rated load torque condition is depicted in Figure 30 which yields a current ripple of 1.5% and the required torque of 11.8 Nm is yielded at the optimal loaded conditions. It is observed that the performance metrics of the hardware prototype SRM are well within the permissible values and provide an optimal electromagnetic performance at the ambient temperature without the saturation of the magnetic core as yielded from the FEM analysis. Hence, the designed SRM yields a high torque and power density suitable for EV applications. The complete design flow involved in achieving a high torque and power density 8/6 SRM with detailed performance metrics used in the design methodology is illustrated in Figure 31.

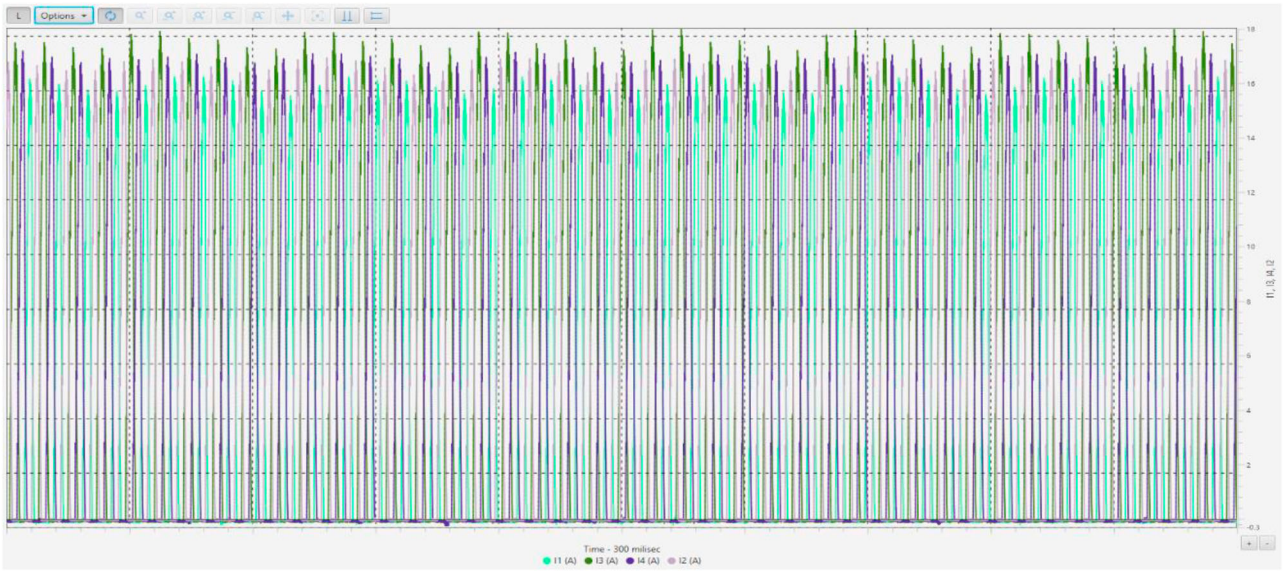

Figure 30. Signals of current sensors at a speed of 3000 rpm at full loaded condition.

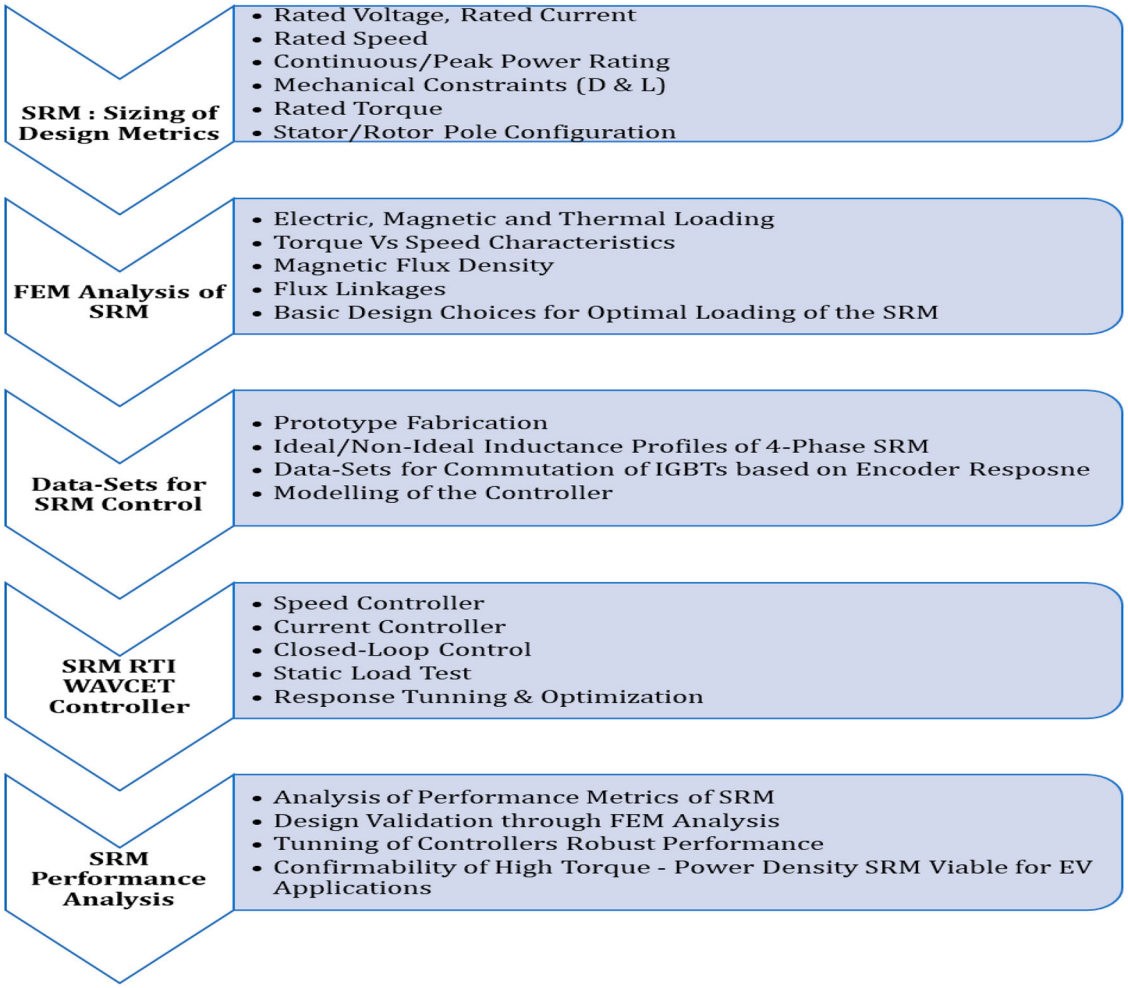

Figure 31. Design methodology of 8/6 SRM for EV application.

8. Conclusion

An 8/6 SRM is considered in this research work as a viable alternative to the existing PMSM/BLDC motors for the automotive traction grade, targeted for the Tri-wheeler E-vehicle applications. In the first stage, the sizing of the mechanical dimensions and power rating of the SRM are validated through the governing equations and the $D \times L$ dimensions are frozen based on the volumetric and diametric constraints by restricting the frame size to 110 mm. In the second stage, the electromagnetic performance metrics of the SRM are predicted and optimized through the FEM analysis. In

the third stage, an FPGA Xilinx-based WAVECT real-time embedded controller is integrated into the SRM through the MATLAB/Simulink platform and control block sets are created for the precise commutation of IGBTs of the classical asymmetric bridge converter based on the real-time response from the interface circuit of the encoder using IR sensors. The entire set-up is subjected to a static load test and the performance metrics are analyzed. The performance metrics of the SRM such as the current ripple less, voltage ripple and mean torque Vs current characteristics with associated torque ripple at the optimal loaded condition conclude the efficacy of the proposed design methodology. The research work concludes that SRM has a great potential to replace the magnetic and induction motors and is best suited for the Tri-wheeler E-vehicle application thereby paving the way for sustainable energy conservation in the automotive sector.

Disclosure statement

No potential conflict of interest was reported by the author(s).

References

[1] Sundaram M, Anand M, Chelladurai J, et al. Design and FEM analysis of high-torque power density permanent magnet synchronous motor (PMSM) for two-wheeler E-vehicle applications. Int Trans Electric Energy Syst. 2022;2022:1–4. doi:10.1155/2022/1217250.

[2] Sundaram M, Chelladurai J, Anand M, et al. Performance evaluation of energy-efficient submersible tubular brushless permanent magnet motor for irrigation application. Arab J Sci Eng. 2022;47(11):14327–14341. doi:10.1007/s13369-022-06744-2

[3] Gan C, Wu J, Sun Q, et al. A review on machine topologies and control techniques for low-noise switched reluctance motors in electric vehicle applications. IEEE Access. 2018;6:31430–31443. doi:10.1109/ACCESS.20/18.2837111

[4] Lan Y, Benomar Y, Deepak K, et al. Switched reluctance motors and drive systems for electric vehicle powertrains: state of the art analysis and future trends. Energies. 2021;14(8):2079. doi:10.3390/en14082079

[5] Han S, Diao K, Sun X. Overview of multi-phase switched reluctance motor drives for electric vehicles. Adv Mech Eng. 2021;13(9):16878140211045195.

[6] Yueying Z, Chuantian Y, Yuan Y, et al. Design and optimisation of an In-wheel switched reluctance motor for electric vehicles. IET Intel Transport Syst. 2019;13(1):175–182. doi:10.1049/iet-its.2018.5097

[7] Sun X, Wan B, Lei G, et al. Multiobjective and multiphysics design optimization of a switched reluctance motor for electric vehicle applications. IEEE Trans Energy Convers. 2021;36(4):3294–3304. doi:10.1109/TEC.2021.3078547

[8] Vuddanti S, Karknalli V, Salkuti SR. Design and comparative analysis of three phase, four phase and six phase switched reluctance motor topologies for electrical vehicle propulsion. Bull Electric Eng Informat. 2021;10(3):1495–1504. doi:10.11591/eei.v10i3.3054

[9] Singh S, Singh HV, Shivshankar C, et al. Design and simulation of 4 kW, 12/8 switched reluctance motor for electric three-wheeler. Mater Today Proc. 2022;65:3461–3475. doi:10.1016/j.matpr.2022.06.057

[10] Bilgin B, Howey B, Callegaro AD, et al. Making the case for switched reluctance motors for propulsion applications. IEEE Trans Veh Technol. 2020;69(7):7172–7186. doi:10.1109/TVT.2020.2993725

[11] Ustkoyuncu N. Application of an in-wheel direct drive motor based on switched reluctance motors for low-power electric vehicles. Sādhanā. 2019;44:1–6. doi:10.1007/s12046-018-0992-x

[12] Yan N, Cao X, Deng Z. Direct torque control for switched reluctance motor to obtain high torque–ampere ratio. IEEE Trans Ind Electron. 2018;66(7):5144–5152. doi:10.1109/TIE.2018.2870355

[13] Reddy PK, Ronanki D, Perumal P. Efficiency improvement and torque ripple minimisation of four-phase switched reluctance motor drive using new direct torque control strategy. IET Electr Power Appl. 2020;14(1):52–61. doi:10.1049/iet-epa.2019.0432

[14] Krishnan R. Switched reluctance motor drives: modeling, simulation, analysis, design, and applications. Boca Raton: CRC Press; 2017.

[15] Rahman KM, Schulz SE. Design of high-efficiency and high-torque-density switched reluctance motor for vehicle propulsion. IEEE Trans Ind Appl. 2002;38(6):1500–1507. doi:10.1109/TIA.2002.805571

[16] Rahman KM, Fahimi B, Suresh G, et al. Advantages of switched reluctance motor applications to EV and HEV: design and control issues. IEEE Trans Ind Appl. 2000;36(1):111–121. doi:10.1109/28.821805

[17] Vijayraghavan P. Design of switched reluctance motors and development of a universal controller for switched reluctance and permanent magnet brushless DC motor drives (PhD diss). Virginia Polytechnic Institute and State University; 2001.

[18] Sundaram M. Development of efficient techniques towards conservation of energy in submersible motor pumps for agriculture and irrigation (PhD diss.). Anna University; 2012.

[19] Dusane PM, Buhr K. Simulation of a brushless dc motor in Ansys–Maxwell 3d. Praga: Mestrado, Czech Technical University; 2016.